Nanostructures

DOI: 10.1002/anie.200903863

Systematic Metal Variation and Solvent and Hydrogen-Gas Storage in Supramolecular Nanoballs**

*Martin B. Duriska, Suzanne M. Neville, Jinzhen Lu, Simon S. Iremonger, John F. Boas, Cameron J. Kepert, and Stuart R. Batten**

Synthetic porous materials, that is, carbon materials, inorganic solids, and coordination polymers (or metal–organic frameworks, MOFs), have been a focus of research for the past few decades, with the goal of enhancing the properties of naturally occurring porous materials (zeolites), which have made a remarkable impact on human society and the environment.[1–3] In more recent times, the focus has shifted towards expanding the applications of synthetic porous metal–organic materials, in particular for gas (i.e., hydrogen, methane, and carbon dioxide) and solvent storage, with promising results.[2,4,5]

Herein we show that discrete metallo-supramolecular materials, as opposed to infinite polymeric systems (including MOFs), are a viable class of porous material for gas and solvent storage.[6] In a recent report we showed the magnetic switching function of a nanoball (Fe-nano).[7] Herein we highlight the versatility of this system through systematic metal and anion variation to form six new analogues of the nanoball, M-nano (M/anion = Cu^{II}/ClO_4^- (Cu-nano), Cu^{II}/BF_4^- (Cu^B-nano), Zn^{II}/ClO_4^- (Zn-nano), Cd^{II}/ClO_4^- (Cd-nano), Fe^{II}/ClO_4^- (Fe^B-nano), Mn^{II}/ClO_4^- (Mn-nano), Figure 1). Furthermore, we demonstrate that the properties of this general system can be extended from magnetic switching to gas and solvent storage, to create a truly multifunctional system. Through parallel thermogravimetric, powder X-ray diffraction, and nitrogen sorption analysis we show that Cu-nano is structurally stable to guest desorption, a property more commonly associated with porous framework materials. Coordinatively unsaturated, accessible Cu^{II} sites are created in this desolvation process, which are of interest for their ability to bind hydrogen gas; it has been shown in a number of nanoporous framework materials that the affinity of hydrogen gas to a surface is greatly increased with the presence of such open metal sites.[5,8,9] Furthermore, using electron paramagnetic resonance (EPR) spectroscopy, we follow the guest exchange and nanostructure functionalization for a range of organic solvents at these bare metal sites.

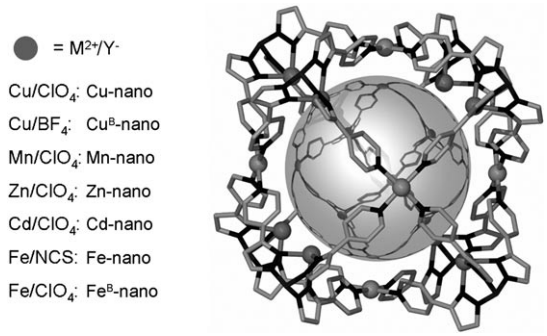

Figure 1. Summary of the M-nano metal(II)/anion analogues.

When utilizing the self-assembly process to construct complex inorganic materials, small variations in synthetic conditions (i.e., metal, pH value, temperature, time, concentration, solvent, anion) often result in large variations in structure and topology; thus, the successful production of families of analogous polymeric (and discrete cage) materials containing different metals is uncommon.[10] The successful synthesis of this family of analogous discrete materials is largely due to the tailored design features of the bifunctional organic ligand $[Tp^{4\text{-py}}]^-$ (tris[3-(4′-pyridyl)pyrazol-1-yl]hydroborate)) and, in particular, to the formation in situ of an intermediate metalloligand building block $[Cu^I(Tp^{4\text{-py}})(MeCN)]$, as outlined in our structural and magnetic report of Fe-nano.[7] Specifically, with the addition of Cu^I to form this metalloligand, the otherwise flexible organic unit is made structurally rigid, and the directionality of the peripheral pyridyl donor groups is effectively locked in. Subsequent addition of a range of divalent metal salts ($[MX_2]$ M^{II} = Cu, Mn, Zn, Cd, Fe, X = ClO_4, NO_3, BF_4) led to self-assembly of analogous nanoball species of the general formula $[(Tp^{4\text{-py}}Cu^IMeCN)_8M^{II}_6(X)_{10}(MeCN)_2](X)_2{\cdot}x\,MeCN$ to produce isostructural crystalline samples in a matter of hours (Figure 1). The structure of each of these species has been confirmed by either single crystal X-ray diffraction[11] or high-resolution powder synchrotron X-ray diffraction,[12] revealing cubic unit cell axes in the range of approximately 61 to 65 Å.

[*] Dr. M. B. Duriska, Dr. S. M. Neville, Dr. J. Lu, Assoc. Prof. S. R. Batten
School of Chemistry, Monash University, Victoria 3800 (Australia)
Fax: (+61) 3-9905-4597
E-mail: stuart.batten@sci.monash.edu.au
Homepage: www.chem.monash.edu.au/staff/sbatten/index.html
Dr. J. F. Boas
School of Physics, Monash University, Victoria 3800 (Australia)
Dr. S. S. Iremonger, Prof. C. J. Kepert
School of Chemistry, University of Sydney, Sydney 2006 (Australia)

[**] We thank the Australian Research Council, the protein crystallography beamline staff at the Australian Synchrotron, the Advanced Photon Source supported by the Australian Synchrotron Research Program, funded by the Commonwealth of Australia under the Major National Research Facilities Program, the National Science Foundation/Department of Energy (HE9522232 and CHE0087817), the Argonne National Laboratory supported by the US Department of Energy, Basic Energy Sciences, Office of Science (DE-AC02-06CH11357) and Drs K. W. Chapman and G. J. Halder for their assistance.

Supporting information for this article is available on the WWW under http://dx.doi.org/10.1002/anie.200903863.

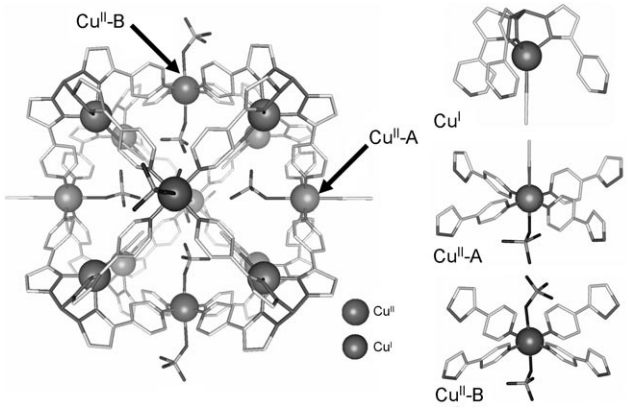

Figure 2. Structural representation of Cu-nano highlighting the Cu^{I}, Cu^{II}-A, and Cu^{II}-B sites and their respective coordination environments, which include either bound perchlorate or acetonitrile molecules.

Taking Cu-nano as a representative example, within each nanoball the Cu^{I} ions are located within the trispyrazole pocket of the scorpionate-type ligand and have their coordination environments completed by one bound acetonitrile molecule each to form neutral $\{Cu^{I}Tp^{4\text{-}py}(MeCN)\}$ moieties (Figure 2). These three-connecting units are bridged by octahedral Cu^{II} ions (in either the $\{Cu^{II}(ClO_4)_2(py)_4\}$ (Cu^{II}-B) or $\{Cu^{II}(ClO_4)(MeCN)(py)_4\}$ (Cu^{II}-A) coordination environment, Figure 2). Thus, discrete units of the general formula $[Cu^{I}_8Tp^{4\text{-}py}_8Cu^{II}_6]$ are formed which are 2.8 nm in diameter (Cu^{II}…Cu^{II} distance). Importantly for the subsequent porous functions of this material, approximately 45% of the Cu^{II} centers per nanoball are in the $\{Cu^{II}(ClO_4)(MeCN)(py)_4\}$ coordination environment, where the bound axial acetonitrile ligands are directed towards the exterior of the nanoball (Figure 2). The replacement of some of the perchlorate anions with neutral acetonitrile ligands also leads to a positive charge on the nanoballs (+8 per three nanoball units). In the crystal lattice, six nanoball units surround a cluster of eight perchlorate anions, which gives rise to an electrostatic interaction that provides robustness to the overall structure (see below and the Supporting Information). Six acetonitrile ligands (from these six nanoball units) are directed into the anionic cluster and are involved in a series of short C–H···O contacts, which create a hydrogen-bonded cage motif of the same topology as the individual nanoballs (see the Supporting Information); thus, an overall cubic 3D network of interactions is attained.

Owing to the relatively crowded internal cavity of the discrete species (Figure 2), we focused on the porous properties and functionalization of the external cavities created through the solid-state packing, which resembles that of ReO_3. This approach is in direct contrast to the majority of other studies on discrete cage-like species, in which the chemical and physical properties of the internal cavities are exploited.[13] Within the crystal lattice of Cu-nano, the packing of the nanoballs and anion clusters results in nanometer-sized (3.5 nm diameter), solvent-filled, cuboctahedral chambers (Figure 3) surrounded by 12 nanoballs. The chambers are interconnected by windows of approximately 1 nm diameter. These interstitial cavities account for approximately 30% of

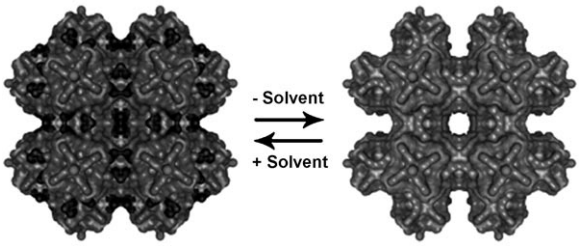

Figure 3. Solvent surface model of the reversible acetonitrile guest (black) removal and addition process within pores generated by the packing of the nanoballs in the crystal lattice of Cu-nano.

the total void volume in the crystal lattice and are filled with disordered acetonitrile molecules. Importantly, these voids, if accessible and stable in the absence of solvent, provide adequate space for gas and solvent storage, reminiscent of porous framework materials.[3,14] Moreover, the surfaces of these pores are lined with potentially labile Cu^{II}-bound acetonitrile molecules, which provide a further means to store solvent or gas but with a more covalent nature, including the possibility of exposing accessible metal sites for greater affinity to gas molecules.[5,8,9,15] The Cu^{II} sites line the surfaces of the windows between the large chambers as well as the smaller spaces between the nanoballs containing the perchlorate/acetonitrile clusters.

Thermogravimetric analysis revealed that these two distinct solvent areas can be targeted individually. In the first step (25–50 °C), the unbound pore solvent is liberated. In the second step (50–75 °C), the Cu^{II}-bound acetonitrile molecules are removed such that bare Cu^{II} sites are exposed (Figure 4a, step A). Importantly, at higher temperatures (75–125 °C) the mass remains stable, indicating thermal stability in

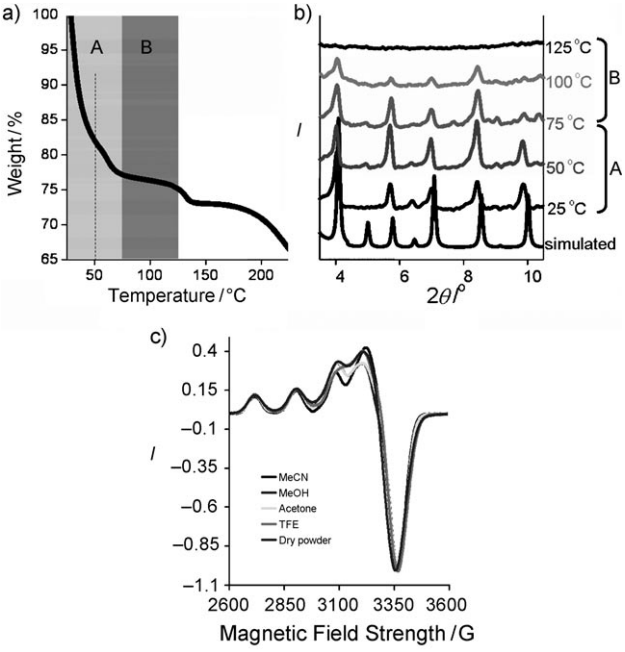

Figure 4. Characterization of Cu-nano. a) Thermogravimetric analysis showing the two-step desolvation process (A and B). b) Variable-temperature powder diffraction analysis. c) EPR spectra (first derivative) of the various solvates at 120 K and microwave frequency 9.43 GHz.

the 'empty' state (Figure 4a, step B). Variable-temperature powder X-ray diffraction measurements in the range 25–125 °C revealed the retention of long-range structural order above 100 °C (Figure 4b). The porous nature of this material was confirmed through N_2 adsorption isotherms at 77 K. The isotherm shows pronounced hysteresis with steps and cannot be readily classified by the IUPAC convention. The hysteresis and steps were fully reproducible and are attributed to percolation effects, whereby the initial adsorption at the constricted pore window restricts further adsorption. Fitting of the adsorption branch to the DFT sorption model gave a pore-size distribution in excellent agreement with the crystallographic model. The Langmuir and BET surface areas were determined to be 1042 and 952 m^3, respectively, which are quite high for metal–organic polyhedra (MOPs).[6,14]

The solvent storage properties of Cu-nano were examined by thermogravimetric vapor resorption analysis, whereby the as-synthesized material was repeatedly heated to desolvation (75 °C) and cooled in the presence of vapors of different organic solvents (acetonitrile, acetone, trifluoroethanol, and methanol). Rapid uptake was observed for each of these solvents. Furthermore, structural analysis was carried out on the solvent-exchanged materials, which allowed successful location of sorbed solvent within the pores; in contrast, the Cu^{II}-bound solvent was unable to be modeled, as these sites are extremely disordered owing to the shared site occupancy with the anions (see the Supporting Information).

To explore changes in the Cu^{II} coordination environments upon guest exchange, EPR measurements in the presence of different solvents were carried out at 120 K. Subtle variations in the Cu^{II} coordination environment, arising from the weak binding of guest molecules, were readily evident. Figure 4c shows an overlay of spectra from the dry powder and the acetonitrile, methanol, acetone, and trifluoroethanol species. These spectra are typical for Cu^{II} in a pseudo-square-planar complex with a different coordination environment along the symmetry axis.[16] Examination of the spin Hamiltonian parameters shows small but significant dependence on the solvent. In particular, the $g_{\|}$ and $A_{\|}$ values for the methanol and acetone species are similar, whereas for acetonitrile $g_{\|}$ is higher and $A_{\|}$ lower, and the reverse is true for trifluoroethanol (see the Supporting Information). Ligand-field considerations place the unpaired electron in an essentially $d_{x^2-y^2}$ orbital with strong σ bonding to the planar ligands. These ligands therefore have the major influence on the EPR spectral parameters. While the planar N-donor ligands here are tightly bound, the ligands along the symmetry axis are only weakly bound (π bonding and distortions from exact square planar give a small admixture of the d_{z^2} orbital into the ground state) and thus have a much smaller influence on the EPR spectra. Indeed, changes of similar magnitude to those found herein have been observed for discrete Cu^{II} complexes in solution.[17]

In recent years it has been demonstrated that crystalline coordination materials of aromatic character with high surface areas and coordinatively unsaturated metal sites are suitable examples for gas storage.[2,3,5,14,18] Since Cu-nano in the "empty" state contains a large surface area lined by aromatic groups and coordinatively unsaturated Cu^{II} sites, it provides a feasible candidate for hydrogen storage. Indeed, hydrogen gas adsorption and desorption isotherms (77 and 87 K) showed an uptake of 1.2 wt.% (at 77 K and 1 bar), equating to approximately 34 hydrogen molecules per nanoball (Figure 5). At 77 K, the maximum loading of H_2 within the sample was extrapolated to be 2 wt.% (ca. 56 H_2 molecules per nanoball). Of particular interest is the calculated enthalpy of adsorption (ΔH_{ads}) at zero loading of 8.75 kJ mol^{-1}, which indicates a relatively strong binding affinity (cf. ca. 5 kJ mol^{-1} for conventional molecular surfaces). ΔH_{ads} values of this magnitude have been shown to be related to interactions between bare metal sites and H_2,[5,9] thus strongly suggesting that such interactions are occurring in this case. This inference is further supported by the abrupt uptake at very low H_2 loadings.

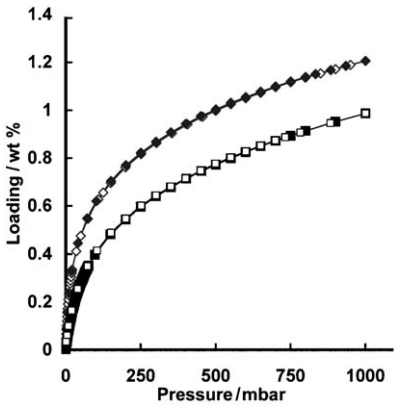

Figure 5. Hydrogen gas adsorption (open symbols) and desorption (filled symbols) isotherms at 77 (diamonds) and 87 K (squares) of Cu-nano.

In summary, we presented an innovative design concept to produce a family of metal-varied discrete cage-like materials that are synthetically directed by the intermediate production of a metalloligand. Such novel methodologies for consistent production of targeted structures are important for the achievement of a range of supramolecular and materials functionalities. Previously, we had shown the magnetic switching ability of the Fe^{II} analogue (Fe-nano), and we now add to this the solvent and hydrogen gas storage ability of the Cu^{II} analogue (Cu-nano). Previous studies into the sorption of hydrogen in polymeric porous materials have shown that different metal species display different affinities towards gas binding.[19] Thus the versatility of the present family allows for the investigation of hydrogen uptake over a range of divalent metal ions within an isomorphous series and the possibility to tune the storage capacity and strength of binding, including possible doping with a second divalent metal for optimization.

Experimental Section

Each of the analogous nanoball materials was synthesized by the same one-pot, two-step method as outlined below for Cu-nano. Firstly, $Cu^{I}(ClO_4)\cdot 4\,MeCN$ (15 mg, 0.046 mmol) was added to a solution of $TlTp^{4\text{-}py}$ (30 mg, 0.046 mmol) in CH_2Cl_2/MeCN (1:1, 5 mL). Then, $Cu(ClO_4)_2\cdot 6\,H_2O$ (13 mg, 0.035 mmol) in MeCN (2 mL)

was added to the resultant bright yellow solution. The dark blue solution was immediately filtered, and the filtrate was allowed to evaporate slowly over the course of one week, after which purple, cube-shaped, X-ray quality crystals were obtained (yield: 30 mg, 87%). Elemental anal. calcd (%) for $C_{208}H_{176}N_{80}O_{48}B_8Cu_{14}Cl_{12}$: C 41.88, H 2.97, N 18.78; found: C 41.80, H 3.22, N 18.67. IR (ATR): $\tilde{\nu}$ = 2253m, 1620s, 1488w, 1465sh, 1432w, 1365w, 1191s, 1106sh, 1050w, 1018s, 843w, 736 cm^{-1} m.

Single-crystal X-ray diffraction was carried out using the high-throughput Protein Crystallography beamline (15.5 keV, 3BM-1) at the Australian Synchrotron. Crystal data for desolvated Cu-nano with adsorbed ethanol (Cu-nano(EtOH)) and trifluoroethanol (Cu-nano-(TFE)) vapor are given in the Supporting Information.

Single-shot powder X-ray diffraction was carried out at the Advanced Photon Source (20.02 keV, 0.61915 Å, 12-BM) at Argonne National Laboratory. Variable-temperature powder X-ray diffraction on Cu-nano was carried out using a Shimadzu S-6000 Diffractometer equipped with $Cu_{K\alpha}$ (λ = 1.5406 Å) radiation (40 kV, 30 mA) in the angle interval 2θ = 2–40° with a step size of 0.02°.

Thermogravimetric analyses were carried out using a TA Instruments Hi-Res TGA 2950 Thermogravimetric Analyzer over the range 25–300 °C for decomposition studies (0.50 °C min^{-1}); for solvent vapor sorption studies, the atmosphere was controlled with a solvent-vapor-filled bubbler equipped with a gas bypass attached to a dry dinitrogen supply (0.1 L min^{-1}), allowing a stream of either dry dinitrogen or solvent vapor/dinitrogen to flow through the system.

Continuous-wave (CW) EPR spectra at X-band frequencies (ca. 9.43 GHz) were obtained with a Bruker ESP380FT/CW spectrometer at 120 K. The microwave frequency was measured with an EIP microwave 548 A frequency counter, and the *g* factors were determined with reference to the F+ line in CaO (2.0001 ± 0.0001).

The adsorption isotherms for N_2 (99.999%) and H_2 (99.999%) were recorded using an Accelerated Surface Area & Porosimetry System (ASAP) 2020 supplied by Micromeritics Instruments Inc. Liquid N_2 and liquid Ar (77.35 and 87.29 K respectively) were used for temperature control.

Received: July 15, 2009
Revised: September 3, 2009
Published online: October 19, 2009

Keywords: hydrogen storage · microporous materials · nanostructures · solvent storage · supramolecular chemistry

[1] L. J. Barbour, *Chem. Commun.* **2006**, 1163; H. K. Chae, D. Y. Siberio-Perez, J. Kim, Y. Go, M. Eddaoudi, A. J. Matzger, M. O'Keeffe, O. M. Yaghi, *Nature* **2004**, *427*, 523; S. Kitagawa, R. Matsuda, *Coord. Chem. Rev.* **2007**, *251*, 2490; J. L. C. Rowsell, O. M. Yaghi, *Microporous Mesoporous Mater.* **2004**, *73*, 3; K. Uemura, R. Matsuda, S. Kitagawa, *J. Solid State Chem.* **2005**, *178*, 2420; O. M. Yaghi, M. O'Keeffe, N. W. Ockwig, H. K. Chae, M. Eddaoudi, J. Kim, *Nature* **2003**, *423*, 705; J. Tian, P. K. Thallapally, S. J. Dalgarno, P. B. McGrail, J. L. Atwood, *Angew. Chem.* **2009**, *121*, 5600 – 5603; *Angew. Chem. Int. Ed.* **2009**, *48*, 5492 – 5495.

[2] D. J. Collins, H. C. Zhou, *J. Mater. Chem.* **2007**, *17*, 3154.

[3] M. J. Rosseinsky, *Microporous Mesoporous Mater.* **2004**, *73*, 15.

[4] S. Takamizawa, *Making Crystals by Design: Nanoporosity, Gas Storage, Gas Sensing*, Wiley-VCH, Weinheim, **2007**; X. Lin, J. Jia, X. Zhao, K. M. Thomas, A. J. Blake, G. S. Walker, N. R. Champness, P. Hubberstey, M. Schröder, *Angew. Chem.* **2006**, *118*, 7518; *Angew. Chem. Int. Ed.* **2006**, *45*, 7358; J. C. Rowsell, E. C. Spencer, J. Eckert, J. A. K. Howard, O. M. Yaghi, *Science* **2005**, *309*, 1350.

[5] M. Dinca, A. Daily, Y. Liu, C. M. Brown, D. A. Neumann, J. R. Long, *J. Am. Chem. Soc.* **2006**, *128*, 16876; L. J. Murray, M. Dinca, J. R. Long, *Chem. Soc. Rev.* **2009**, *38*, 1294.

[6] H. Furukawa, J. Kim, N. W. Ockwig, M. O'Keeffe, O. M. Yaghi, *J. Am. Chem. Soc.* **2008**, *130*, 11650.

[7] M. B. Duriska, S. M. Neville, B. Moubaraki, J. D. Cashion, G. J. Halder, K. W. Chapman, C. Balde, J.-F. Létard, K. S. Murray, C. J. Kepert, S. R. Batten, *Angew. Chem.* **2009**, *121*, 2587; *Angew. Chem. Int. Ed.* **2009**, *48*, 2549.

[8] Y.-G. Lee, H. R. Moon, Y. E. Cheon, M. P. Suh, *Angew. Chem.* **2008**, *120*, 7855 – 7859; *Angew. Chem. Int. Ed.* **2008**, *47*, 7741 – 7745.

[9] V. K. Peterson, Y. Liu, C. M. Brown, C. J. Kepert, *J. Am. Chem. Soc.* **2006**, *128*, 15578.

[10] S. Hiraoka, K. Harano, M. Shiro, Y. Ozawa, N. Yasuda, K. Toriumi, M. Shionoya, *Angew. Chem.* **2006**, *118*, 6638; *Angew. Chem. Int. Ed.* **2006**, *45*, 6488.

[11] M-nano crystal data: Cu-nano: $C_{378}H_{225}B_{12}C_{122}Cu_{21}N_{147}O_{94}$, M_r = 10574.01, purple cube, cubic, space group $Fm\bar{3}c$ (no. 130), a = 62.518(7) Å, V = 244352(47) Å^3, T = 100 K, ρ_{calcd} = 1.150 g cm^{-3}, $\mu(Mo_{K\alpha})$ = 0.879 mm^{-1}, GOF = 2.123, R_1 for $I > 2\sigma(I)$: 0.1357, wR_2 for all data: 0.4110. Cu^B-nano: $C_{360}H_{261}B_{31}Cu_{21}F_{88}N_{147}O_{10}$, M_r = 10147.61, green-blue cube, cubic, space group $Fm\bar{3}c$ (no. 130), a = 62.178(7) Å, V = 240387(48) Å^3, T = 100 K, ρ_{calcd} = 1.122 g cm^{-3}, $\mu(MoK_\alpha)$ = 0.806 mm^{-1}, GOF = 1.533, R_1 for $I > 2\sigma(I)$: 0.1191, wR_2 for all data: 0.3413. Zn-nano: $C_{366}H_{261}B_{12}C_{113}Cu_{12}N_{147}O_{74}Zn_9$, M_r = 9843.60, colorless cube, cubic, space group $Fm\bar{3}c$ (no. 130), a = 62.688(7) Å, V = 246350(5) Å^3, T = 100 K, ρ_{calcd} = 1.062 g cm^{-3}, $\mu(Mo_{K\alpha})$ = 0.867 mm^{-1}, GOF = 1.064, R_1 for $I > 2\sigma(I)$: 0.0815, wR_2 for all data: 0.2416. Fe^B-nano: $C_{342}H_{297}B_{12}Cl_{22}Fe_{21}N_{135}O_{94}$, M_r = 9884.62, yellow cube, cubic, space group $Fm\bar{3}c$ (no. 130), a = 61.197(7) Å, V = 229187(46) Å^3, T = 100 K, ρ_{calcd} = 1.146 g cm^{-3}, $\mu(Mo_{K\alpha})$ = 0.685 mm^{-1}, GOF = 2.219, R_1 for $I > 2\sigma(I)$: 0.1559, wR_2 for all data: 0.4414. CCDC 738378 (Cu^B-nano), 738379 (Cu-nano-(EtOH)), 738380 (Cu-nano), 738381 (Cu-nano(TFE)), 738382 (Fe^B-nano), and 738383 (Zn-nano) contain the supplementary crystallographic data for this paper. These data can be obtained free of charge from The Cambridge Crystallographic Data Centre via www.ccdc.cam.ac.uk/data_request/cif.

[12] M-nano powder synchtrotron X-ray diffraction Le Bail refined unit cell parameters: Cu-nano: a = 61.789(3) Å, V = 235914(3) Å^3, Cu^B-nano: a = 61.789(3) Å, V = 235911(3) Å^3, Cd-nano: a = 65.118(2) Å, V = 276126(4) Å^3, Zn-nano: a = 61.827(4) Å, V = 236339(3) Å^3, Fe-nano: a = 64.713(4) Å, V = 271008(3) Å^3, Mn-nano: a = 64.887(3) Å, V = 273199(2) Å^3.

[13] M. Fujita, D. Oguro, M. Miyazawa, H. Oka, K. Yamaguchi, K. Ogura, *Nature* **1995**, *378*, 469; M. Tominaga, K. Suzuki, T. Murase, M. Fujita, *J. Am. Chem. Soc.* **2005**, *127*, 11950; M. Yoshizawa, Y. Takeyama, T. Kusukawa, M. Fujita, *Angew. Chem.* **2002**, *114*, 1403; *Angew. Chem. Int. Ed.* **2002**, *41*, 1347.

[14] N. L. Rosi, J. Eckert, M. Eddaoudi, D. T. Vodak, J. Kim, M. O'Keeffe, O. M. Yaghi, *Science* **2003**, *300*, 1127.

[15] K. W. Chapman, P. J. Chupas, E. R. Maxey, J. W. Richardson, *Chem. Commun.* **2006**, 4013.

[16] J. Peisach, W. E. Blumberg, *Arch. Biochem. Biophys.* **1974**, *165*, 691; J. R. Pilbrow, *Transition Ion Electron Paramagnetic Resonance*, Clarendon Press, Oxford, **1990**.

[17] S. Antosik, N. M. D. Brown, A. A. McConnell, A. L. Porte, *J. Chem. Soc. A* **1969**, 545.

[18] M. Latroche, S. Surble, C. Serre, C. Mellot-Drazneiks, P. L. Llewellyn, J.-H. Lee, J.-S. Chang, S. H. Jhung, G. Ferey, *Angew. Chem.* **2006**, *118*, 8407; *Angew. Chem. Int. Ed.* **2006**, *45*, 8227.

[19] K. W. Chapman, P. D. Southon, C. L. Weeks, C. J. Kepert, *Chem. Commun.* **2005**, 3322.

